Available online at www.sciencedirect.com

SciVerse ScienceDirect

Ceramics International 38 (2012) 4791–4796

CERAMICS INTERNATIONAL

www.elsevier.com/locate/ceramint

The photo-catalytic activities of neodymium and fluorine doped TiO_2 nanoparticles

Lu Yang [a,b], Peng Liu [b,*], Xi Li [b], Song Li [c]

[a] State Key Laboratory of Silicate Materials for Architectures, Wuhan University of Technology, Wuhan 430070, PR China
[b] Department of Chemistry, School of Sciences, Wuhan University of Technology, Wuhan 430070, PR China
[c] School of Logistics Engineering, Wuhan University of Technology, Wuhan 430070, PR China

Received 9 January 2012; accepted 21 February 2012
Available online 3 March 2012

Abstract

A series of photo-catalysts were synthesized by neodymium and fluorine doped TiO_2, and their characteristics evaluated by X-ray diffraction (XRD), UV–vis diffuse reflectance spectra (UV–vis), scanning electron microscopy (SEM), and energy dispersive X-ray spectroscopy (EDS). Neodymium and fluorine doped TiO_2 has obvious absorption in the visible light and the absorption edge shifts toward red wavelength. In addition, compared with pure TiO_2, the doped catalyst has intense absorption at 528, 587, 750, 808, and 881 nm. The catalytic efficiency was tested by monitoring the photo-catalytic degradation of methylene blue (MB) in visible light and ultraviolet light. The results showed that the optimum doping content was Nd:F:TiO_2 = 0.5:5:100 (molar ratio) heat treated at 500 °C, and the reaction rates of MB degradation were estimated to be about 1.76 times and 1.45 times higher than undoped TiO_2 in ultraviolet light and visible light.

Keywords: Doped TiO_2; Photo-catalysis; Ultraviolet light; Visible light; Methylene blue

1. Introduction

TiO_2 has many advantages, such as stability, non-toxicity, intense photo catalysis and low price [1–3], these advantages let it has been widely used in water and air purification, antibiosis ceramics, solar cells and so on. This material usually has three crystal forms: rutile, anatase, and brookite [4]. The anatase form usually has more efficient in photo-activity than rutile and brookite [5–7]. However, the band gap of anatase (3.2 eV) is not handled easily for solar applications, which limits wide application in visible range. In recent years, in order to decrease the band gap energy, many methods have been attempted to improve the photo-catalysis efficiency, such as nonmetal and metal doping. Those methods created intra-band-gap states close to the conduction or valence band edges and hence induce visible light absorption at the sub-band-gap energies [8]. Up to date, there are two ways for metal doping: doping of transition metal and doping of rare earth metal. Transition metal dopants in TiO_2 can improve the trapping of electrons and inhibit e^-–h^+ recombination [9]. Some transition metals doping produced a doping energy level, which capture the electrons and holes. So the lower energy photon (visible light) can motivate it. But this method has not been commercialized successfully, because their low quantum yield in liquid phase photo catalytic system, the quantum yield of it is very low and seldom exceeds 1% [10].

Because rare earth elements have fecundity energy level and 4*f* electron transitions, they can easily produce multiple electron configurations which are of special optical properties. Recently, Xu [11] and Stengl [12] systematically reported the rare earth elements doped TiO_2. According to their and previous studies, rare earth elements doping can improve the surface adsorption of the catalyst. These materials can be excited by visible light, and the electron–hole recombination is prevented. Interestingly, TiO_2 doped with Nd^{3+} has many absorption peaks in the range of visible-light wavelength (at 431, 474, 527, 582, 747 and 805 nm wavelength). Those peaks are attributed to the 4*f* electron transitions of the ions [12,13]. However, the absorption at 400–550 nm (431, 474, 527 nm) was very weak, therefore the absorption of the sun light by Nd^{3+} doped TiO_2 was unavailable in these wavelengths.

* Corresponding author. Tel.: +86 27 63410197; fax: +86 27 87863157.
E-mail address: xiaoqiyeting@163.com (P. Liu).

0272-8842/$36.00
doi:10.1016/j.ceramint.2012.02.067

TiO_2 doped with nonmetal such as N [14], S [15], C [16], I [17], and F [18–21], has also been investigated by various research groups. All of them can increase the photo-catalytic activity of TiO_2. Particularly, F doped TiO_2 could shift the optical absorption edge toward lower energy and thus enhance the photo-catalytic activity [19]. Recently, Zhao [20] and He [21] suggested that, by modification with a nonmetal and a metal oxide, the doped TiO_2 not only can be excited with visible light, but also its catalytic activity was enhanced.

In our paper, we reported the preparation and characterization of neodymium and fluoride doped TiO_2. At the same time, its catalytic efficiency was also studied in detail on MB (methylene blue). In order to evaluate the photo-catalytic activity of the catalyst in different situations, we chose two types of light source (ultraviolet light and visible light) to serve as a model system, respectively. Through UV–vis spectrophotometer and optical filter, different photo-effect and mechanism were analyzed.

2. Materials and methods

2.1. Materials

Tetrabutyl titanate, ammonium fluoride, neodymium nitrate, ethanol, acetic acid glacial, methylene blue (MB), and other routine chemicals were purchased from Shenshi Chem. All chemicals were analytical grade. Doubly distilled water was used in all experiments.

2.2. Preparation of photo-catalysts

The doped TiO_2 particles were prepared by the sol–gel route. In the molar ratio $Ti(OBu)_4$:C_2H_5OH:CH_3COOH:H_2O = 1:18:2:5, 9.5 ml $Ti(OBu)_4$ was dissolved in the solution that contain 19 ml C_2H_5OH, 3.2 ml CH_3COOH, and different quantity of neodymium nitrate, and then stirred for 30 min, This solution was marked solution A. Solution B contained 10 ml C_2H_5OH, 2.5 ml H_2O, and 0.0515 g NH_4F. B was slowly added into A, and then the mixture hydrolyzed at 303 K for 30 min under vigorous stirring, and finally the sol obtained. The gel was prepared by aging the sol 24 h at room temperature. And then the derived gel dried at 373 K for 12 h to remove the solvent and heat treated at different temperatures (400, 500, 600 °C) for 3 h and milled into powders. For comparison, different samples with varying the quantity of neodymium nitrate (9.181×10^{-3}, 4.591×10^{-2}, 9.181×10^{-2} g) were synthesized and pure TiO_2 was prepared in the same way. The samples denoted as TiF_5Nd_m-n00 °C (m stand for the different mass of neodymium nitrate and n stand for the first word of calcined temperature).

2.3. Characterization

2.3.1. X-ray diffraction (XRD) analysis

The crystalline phase that evolved after calcinations of the powders was determined by XRD (PHILIPS P W 3O4O/60X'PertPRO) using a Cu Kα ray source at the scanning speed of 8° min^{-1} and scanning range from 20° to 70°. The mean crystallite diameters were estimated by application of the Scherrer equation.

2.3.2. UV–vis diffuse reflectance analysis

UV–vis diffuse reflectance spectra for evaluation of photophysical properties were recorded in the diffuse reflectance mode (R) and transformed to absorption spectra through the Kubelka–Munk function [22]. A Lambda 35 (PerkinElmer) spectrometer equipped with a Labsphere RSA-PE-20 integration sphere and with MgO as a standard used.

2.3.3. SEM and EDS analysis

The morphology of sample was observed by SEM (JEOL JSM-5610LV), and energy dispersive spectroscopy (EDS) was recorded on JSM-5610LV as its accessory.

2.4. Photo-catalytic activity testing

2.4.1. Visible light induced

The visible light photo-catalytic activity of the catalysts was evaluated by using methylene blue (MB) in a glass container. The visible light source was a metal halide lamp (150 W, UYU lighting), a long-pass glass filter with 400 nm and heat insulating glass (wavelength $\leq$ 800 nm) were employed to evaluate the photo-catalytic activity of products in visible light range and remove the effect of heat. The distance between the lamp and the reaction liquid was 12 cm, and the reaction liquid was prepared by mixing 0.03 g catalysts and 60 ml MB aqueous solution (10 mg/L). Then the suspension was stirred in the dark for 30 min to reach adsorption equilibrium before irradiation. Then the mixture was irradiated by the light. After 30 min, 5 ml of suspension was taken from the mixture and centrifuged at 4000 rpm to separate the photo-catalyst particles, and then the supernatants were analyzed by UV–vis spectrophotometer (721, Shanghai 3rd Analytical Instrument Ltd.). Subsequently, readings were taken in 30 min intervals. All the experiments were performed three times and the data are given as the arithmetic mean standard deviation (n = 3).

The degradation rate and reaction rate were calculated by as following formulas:

$$\omega\% = \frac{c}{c_0} \tag{1}$$

$$\mathrm{Ln}\frac{c}{c_0} = -kt \tag{2}$$

where c and c_0 are the concentrations of the primal and remaining MB, k is the reaction rate, and t is the light application time.

2.4.2. Ultraviolet light induced

For ultraviolet light photo-catalytic activity of the catalysts, the same procedures were performed with Section 2.4.1 except that the long-pass glass filter with 400 nm was exchanged by uviol glass filter (wavelength $\leq$ 400 nm). All the experiments were performed three times and the data are given as the arithmetic mean standard deviation (n = 3).

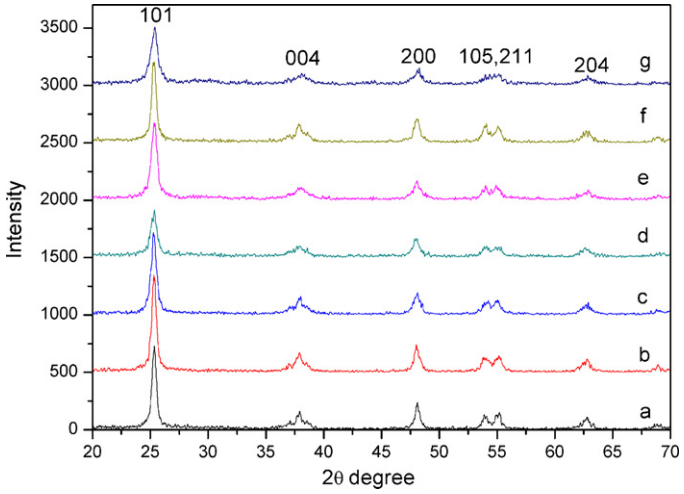

Fig. 1. XRD patterns of doped TiO_2 samples denoted as (a) undoped TiO_2-5, (b) TiF_5-5, (c) $TiF_5Nd_{0.1}$-5, (d) $TiF_5Nd_{0.5}$-4, (e) $TiF_5Nd_{0.5}$-5, (f) $TiF_5Nd_{0.5}$-6, and (g) TiF_5Nd_1-5.

3. Result and discussion

3.1. Physical properties of TiO_2 photo-catalysts

3.1.1. XRD analysis

Fig. 1 shows that the XRD patterns of the Nd, F doped TiO_2 with various doping contents and pure TiO_2 calcined at different temperatures. The peaks at 2θ values showed that all products were anatase crystal, no rutile was observed and no Nd and F element peak was found in the XRD patterns (PDF 21-1272). The peak at 25.4° was used to calculate the average crystal size by Scherrer equation [23]:

$$D = \frac{0.89\lambda}{\beta \cos\theta} \quad (3)$$

where D is the average size of the particle, λ is the wavelength of X-ray radiation, β is the full width at half maximum, and θ is the diffraction angle.

The crystal sizes of all samples are shown in Table 1. In Fig. 1 and Table 1, from (a) to (b), the average sizes increased at the same calcined temperature. The similar consequence was reported by Trapalis [19] and Yu [24]. The reason was that the fluorine ion doping easily entered the TiO_2 lattice (fluorine ion radii are similar to oxygen ion) and simultaneously initiated the crystallization process. From Fig. 1, it can be observed that with the Nd doping increased from 0.1% to 1%, the crystallite size decreased obviously (Fig. 1 and Table 1). This can be attributed to the presence of Nd–O–Ti in doped samples, which inhibits the growth of crystal grains [25]. Moreover, with the increase of heat-treat temperature, the crystallite size also increased, as shown in Fig. 1 and Table 1. The reason was that the surface energy of particles enhanced dramatically with the increase of temperature, in order to decrease the surface energy and maintaining stability, the particles coagulated and the size increased.

Table 1
Photocatalyst properties of doped-TiO_2 and pure TiO_2 samples XRD results.

Mole ratio of Nd:F:TiO_2	Calcination temperature (°C)	The peak half-width (°)	Crystallite size (nm)
0:0:100	500	0.45883	17.5
0:5:100	500	0.44914	17.9
0.1:5:100	500	0.54281	14.8
0.5:5:100	400	–	–
0.5:5:100	500	0.59749	13.4
0.5:5:100	600	0.46653	17.2
1:5:100	500	0.68114	11.8

3.1.2. UV–vis diffuse reflectance analysis

Fig. 2 shows UV–vis diffuse reflectance spectra of pure TiO_2 and doped TiO_2 with different doping contents (molar ratios) heat treated at the same temperature. All doped TiO_2 has obvious absorption in the visible light compared with pure TiO_2. When the content of Nd increased from 0.1% to 0.5%, the absorption in ultraviolet region slightly decreased and in visible light region increased. Especially, at 528(1), 587(2), 750(3), 808, 881 nm (808 and 881 nm are not shown herein) there have intense absorption compared with pure TiO_2. This manifestation results from the Nd's characteristic 4*f* electron transitions [13]. Furthermore, when the contents of Nd increased from 0.5% to 1%, the absorption in ultraviolet region and visible light region decreased significantly; this may be caused by the fact that excessive Nd_2O_3 was on the surface of the particle, which detrimentally affected the F species on the surface of the products. Fig. 2 shows that the calcination temperature has also influence on the absorption in the visible light region.

Furthermore, the absorption edge shifted toward red wavelengths for all doped TiO_2 as shown in Fig. 3, the plot of the Kubelka–Munk functions ($F(R)$) against the photon energy (E_{ph}) [26,27]. The equation is that

$$A = \log\left(\frac{1}{R_\infty}\right) \quad (4)$$

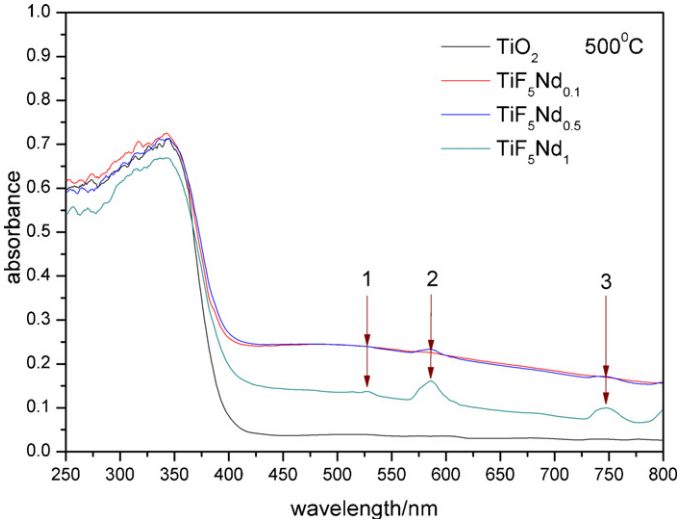

Fig. 2. UV–vis diffuse reflectance spectra of pure TiO_2 and Nd:F:TiO_2 with different doping contents (molar ratios) calcined at the same temperature.

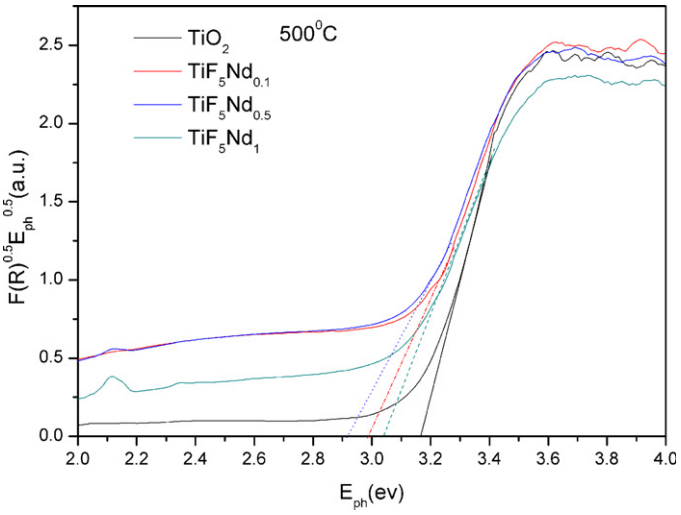

Fig. 3. The band gaps of pure TiO_2 and Nd:F:TiO_2 with different doping contents (molar ratios) calcined at the same temperature.

$$F(R) = \frac{(1 - R_\infty)^2}{2R_\infty} \quad (5)$$

$$E_{ph} = \frac{1240}{\lambda} \quad (6)$$

where A is a absorbance, R_∞ is the reflectance of samples in infinite thick, $F(R)$ is the Kubelka–Munk functions, E_{ph} is the photon energy, and λ is the wavelength. The band gap energies of all samples were calculated by preceding formulas, the results were that 3.17, 3.04, 2.98, 2.91 eV for TiO_2, TiF_5Nd_1, $TiF_5Nd_{0.1}$, $TiF_5Nd_{0.5}$, respectively. These consequences indicated that the absorbance edge of $TiF_5Nd_{0.5}$ shifted significantly to the visible region in all doped samples. The reason was that Ti^{4+} entered Nd_2O_3 during heat treatment (the ionic radius of Nd^{3+} (0.0983 nm) is much larger than Ti^{4+} (0.068 nm), Nd^{3+} cannot replace the Ti^{4+} in TiO_2 crystal lattice), which made the Ti^{4+} into Ti^{3+}. Furthermore, fluorine ion replaced oxygen ion (the ionic radius of F^- and O^{2-} are similar), and created a charge imbalance, which made more Ti^{3+} active sites [28]. Nd and F doping also produced oxygen vacancies on the surface of TiO_2, hence, a quantity of Ti^{3+} and oxygen vacancies made the band gap shifts in the visible light region.

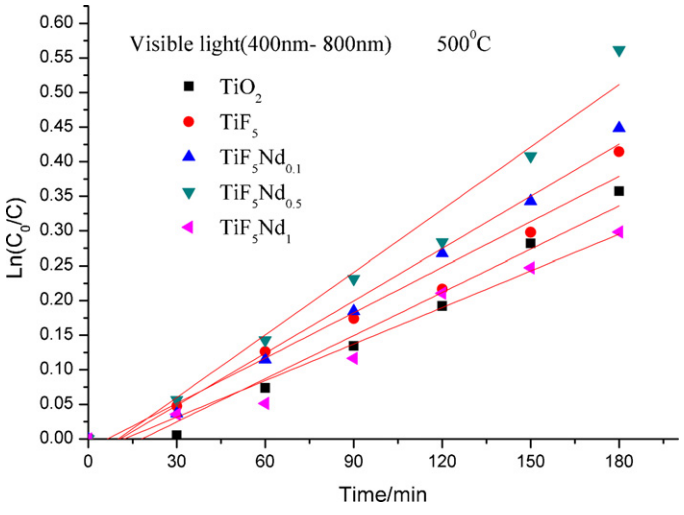

Fig. 5. Photo catalytic degradation rate of MB in visible light using pure TiO_2 and Nd:F:TiO_2 with different molar ratios calcined at 500 °C.

3.1.3. SEM and EDS analysis

Fig. 4 shows the SEM image and EDS spectrum of $TiF_5Nd_{0.5}$-500. It can be observed that the doped TiO_2 mainly presented in the form of glomeration, and the size of the glomeration was about 50–100 nm. EDS spectrum result indicated that there were F and Nd elements in the sample.

3.2. Photo catalytic activity testing

3.2.1. Visible light induced

Fig. 5 shows the photo-catalytic degradation rate of MB using pure TiO_2 and Nd, F doped TiO_2 with diverse doping contents (500 °C) in visible light. Fig. 6 shows the influence of calcination temperature on photo-catalytic degradation rate of MB. MB is a heterocyclic aromatic chemical compound. It has many uses in a range of different fields, such as biology and chemistry. It can also be used as a test molecular for measuring the catalysis efficiency. In Figs. 5 and 6, it can be seen MB was degraded gradually in the presence of catalysts under the illumination. The most efficient catalyst to degrade MB was Nd combined with F doped TiO_2 with molar ratio of 0.5:5:100. The reaction rate was estimated to be about 1.45 times higher

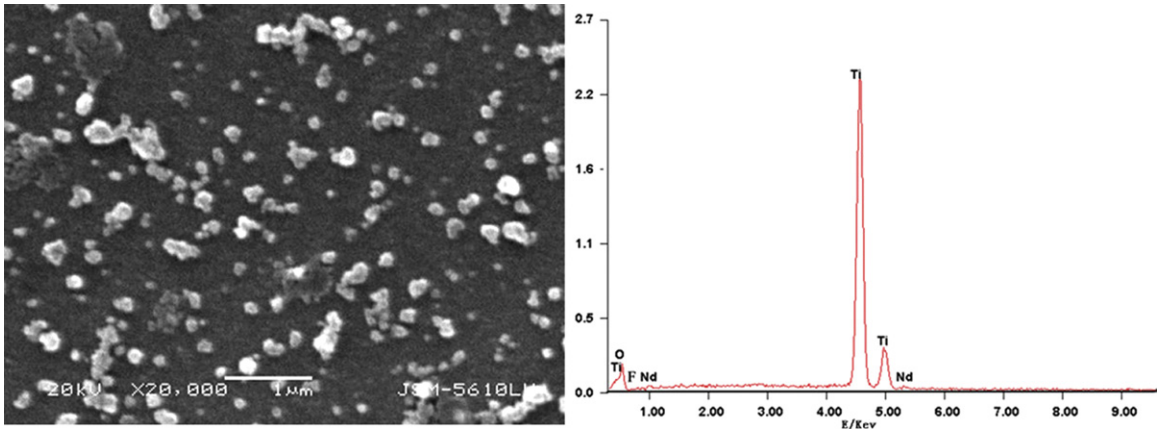

Fig. 4. SEM images and EDS spectrum of $TiF_5Nd_{0.5}$-500.

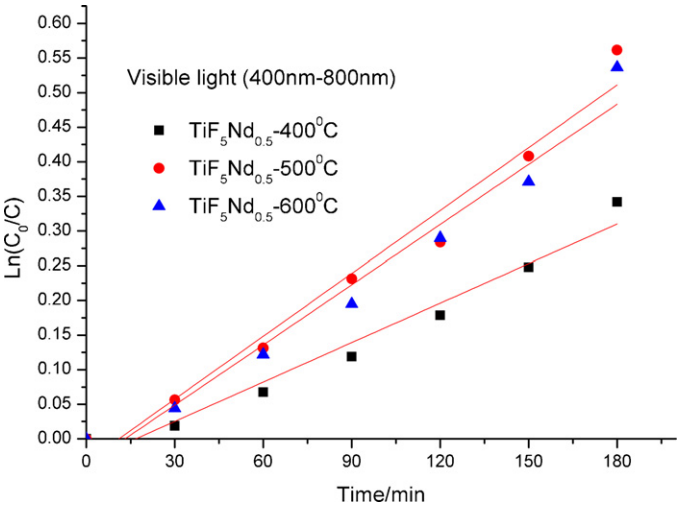

Fig. 6. Photo catalytic degradation rate of MB in visible light using Nd:F:TiO_2 = 0.5:5:100 (molar ratio) calcined at different temperatures.

than undoped TiO_2 (the reaction rates of MB with all samples are shown in Table 2). Moreover, with the increase of Nd, the photo-catalysis activity of products increased at first (0.1–0.5%) and then decreased (0.5–1%). The above results can be explained as following: the aromatic chemical compound is very non-active. However, with the attack of free radical, the aromatic ring could be destroyed in short time. When the visible light illuminated the doped sample, the electron can be excited from valance band of samples and moved to the surface, meanwhile, the hole left in the conduct band of the samples. The electron and hole have almighty reduction and oxidation capacity [29], However, that process was accompanied by recombination of electron–hole pairs, and hence it resulted low photo-catalysis efficiency. Those weaknesses can be compensated by rare earth elements doping. Certain amount of Nd_2O_3 on the surface of TiO_2 separated charge carriers efficiently, prolonged the lifetime of carriers, and inhibited the recombination of electron–hole pairs, with the Nd doping content exceed a certain point, excessive Nd_2O_3 coating on the surface of TiO_2 would inhibit the adsorption of MB and decreased the absorption in light, and thus decreased the photo-catalytic activity. Moreover, F doping also promoted the photo catalytic activity of TiO_2. According to Li [30] and Di Valentin [31], F^- could substitute O^{2-} formed F–Ti construction, which produce more Ti^{3+} active sites. At the same time, when TiO_2 doped with fluorine, high density localized levels appeared below the valance band, which was mainly composed of an F_{2p} state [32]. This process promoted the oxidation potential of the sample. Due to cooperative effects of neodymium and fluorine, the photo-catalytic activity to MB increased dramatically. Besides, the absorption in visible light region and dye sensitization also promoted the photo-catalytic activity of doped TiO_2 [33].

Table 2
The reaction rates and relativity of MB using all sample in bi-light source.

Sample	Reaction rates (k, min^{-1})	Relativity (R)	Light source
TiO_2-5	2.08×10^{-3}	0.98	Visible light
	5.19×10^{-3}	0.99	Ultraviolet light
TiF_5-5	2.18×10^{-3}	0.99	Visible light
$TiF_5Nd_{0.1}$-5	2.51×10^{-3}	0.99	Visible light
$TiF_5Nd_{0.5}$-4	1.90×10^{-3}	0.98	Visible light
$TiF_5Nd_{0.5}$-5	3.02×10^{-3}	0.98	Visible light
	9.14×10^{-3}	0.99	Ultraviolet light
$TiF_5Nd_{0.5}$-6	2.90×10^{-3}	0.98	Visible light
TiF_5Nd_1-5	1.76×10^{-3}	0.98	Visible light

The influence of calcination temperature on photo-catalytic degradation rate of MB is shown in Fig. 6. With the increase of the calcination temperature, the efficiency of Nd and F doped TiO_2 increased and then decreased. The result suggested that at 500 °C the degree of crystalline was better than 400 °C; this can be proved by XRD. However, when the calcination temperature continued to increase (600 °C), the doped TiO_2 has bigger size compared with the doped TiO_2 heat treated at (500 °C), therefore, it could not absorb more MB [34] and thus resulted in a lower photo catalytic activity (the reaction rates of MB with all samples are shown in Table 2).

3.2.2. Ultraviolet light test

Fig. 7 shows the photo-catalytic degradation rate of MB using $TiF_5Nd_{0.5}$-5 in UV-light. It can be seen that the photo catalysis effect of doped TiO_2 was enhanced compared with pure TiO_2 after irradiation for 120 min, and the reaction rate of MB over $TiF_5Nd_{0.5}$-5 was estimated to be about 1.76 times higher than undoped TiO_2 (the reaction rates of MB with all samples are shown in Table 2). This result can be explained as follows: for pure TiO_2 or doped TiO_2, e^- in the VB will be easily excited to CB under UV light irradiation and the h^+ left in the VB. e^- can combine with oxygen to form superoxide anions and h^+ can oxidize hydroxyl and water to give hydroxyl radicals ($^{\bullet}OH$), superoxide anions and hydroxyl radical degraded the organic pollutant [35]. However, this process was accompanied by recombination of electron–hole pairs which results in low photo-catalysis efficiency [36]. But doped TiO_2 ($TiF_5Nd_{0.5}$-5) can prolong this recombination process and promote the oxidation capability compared to pure TiO_2.

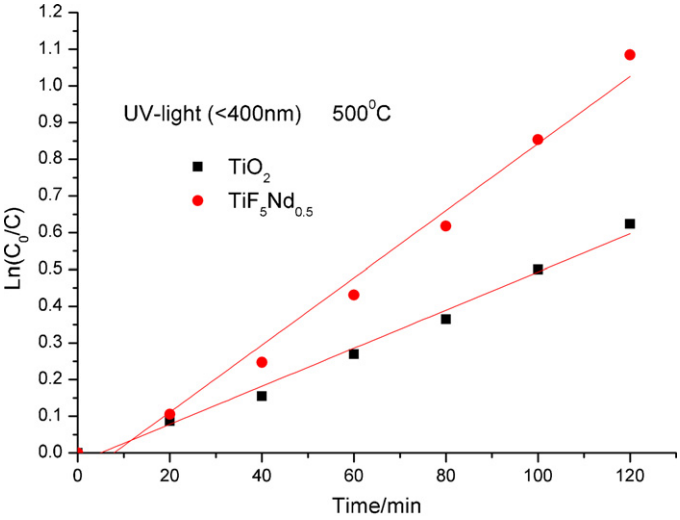

Fig. 7. Photo catalytic degradation rate of MB in UV-light using pure TiO_2 and $TiF_5Nd_{0.5}$ calcined at 500 °C.

4. Conclusions

In this study, we have synthesized and characterized neodymium and fluorine doped TiO_2 nanoparticles. UV–vis spectra showed that neodymium and fluorine doped TiO_2 has obvious absorption in the visible light and the absorption edge shifts toward red wavelengths. It also has intense absorption compared to pure TiO_2 at 528, 587, 750, 808, 881 nm. This phenomenon can be attributed to Nd and F doping. The results of photo-catalysis of MB suggested that the optimal sample was $TiF_5Nd_{0.5}$-5. And the reaction rates of MB were estimated to be about 1.76 times and 1.45 times higher than undoped TiO_2 in ultraviolet light and visible light, respectively. This co-doping effect promoted the photo-catalytic activity in both UV and visible region.

Acknowledgments

We gratefully acknowledge the financial support of the Fundamental Research Funds for the Central Universities (2011-Ia-035) and National Natural Science Foundation of China (No. 51175394).

References

[1] M.R. Hoffmann, S.T. Martin, W.Y. Choi, D.W. Bahnemann, Environmental applications of semiconductor photocatalysis, Chem. Rev. 95 (1995) 69–96.
[2] L. Zang, C. Lange, I. Abraham, S. Storck, W.F. Maier, H. Kisch, Amorphous microporous titania modified with platinum(IV) chloride, J. Phys. Chem. B 102 (1998) 10765–10771.
[3] K.M. Parida, B. Naik, Synthesis of mesoporous TiO_2–xNx spheres by template free homogeneous co-precipitation method and their photocatalytic activity under visible light illumination, J. Colloid Interface Sci. 333 (2009) 269–276.
[4] A.F. Wells, Structural Inorganic Chemistry, Clarendon Press, Oxford, 1975.
[5] K. Nagaveni, G. Sivalingam, M.S. Hegde, G. Madras, Photocatalytic degradation of various dyes by combustion synthesized nano anatase TiO_2, Appl. Catal. B 45 (2003) 23–38.
[6] O. D'Hennezel, D.F. Ollis, Surface prechlorination of anatase TiO_2 for enhanced photo-catalytic oxidation of toluene and hexane, Helv. Chim. Acta 84 (2001) 3511–3518.
[7] G.S. Li, L.P. Li, J. Boerio-Goates, B.F. Woodfield, High purity anatase TiO_2 nanocrystals: near room-temperature synthesis, grain growth kinetics, and surface hydration chemistry, J. Am. Chem. Soc. 127 (2005) 8659–8666.
[8] W.Y. Su, J.X. Chen, L. Wu, X.C. Wang, X.Z. Fu, Visible light photocatalysis on praseodymium(III)-nitrate-modified TiO_2 prepared by an ultrasound method, Appl. Catal. B: Environ. 77 (2008) 264.
[9] J.K. Zhou, Y.X. Zhang, X.S. Zhao, A.K. Ray, Photodegradation of benzoic acid over metal-doped TiO_2, Ind. Eng. Chem. Res. 45 (2006) 3503–3511.
[10] M.I. Litter, J.A. Navio, Photocatalytic properties of iron-doped titania semiconductors, J. Photochem. Photobiol. A: Chem. 98 (1996) 171–181.
[11] A.W. Xu, Y. Gao, H.Q. Liu, The preparation, characterization, and their photocatalytic activities of rare-earth-doped TiO_2 nanoparticles, J. Catal. 207 (2002) 151–157.
[12] V. Stengl, S. Bakardjieva, N. Murafa, Preparation and photocatalytic activity of rare earth doped TiO_2 nanoparticles, Mater. Chem. Phys. 114 (2009) 217–226.
[13] H.M. Crosswhite, B.H. Dieka, W.J. Carter, Free-ion and crystalline spectra of Pr3+ (Pr IV), J. Chem. Phys. 43 (1965) 2047.
[14] R. Asahi, T. Morikawa, T. Ohwaki, K. Aoki, Y. Taga, Visible-light photocatalysis in nitrogen-doped titanium oxides, Science 293 (2001) 269–271.
[15] J.C. Yu, W. Ho, J. Yu, H. Yip, P.K. Wong, J. Zhao, Efficient visible-light-induced photocatalytic disinfection on sulfur-doped nanocrystalline titania, Environ. Sci. Technol. 39 (2005) 1175.
[16] S. Sakthivel, H. Kisch, Daylight photocatalysis by carbon-modified titanium dioxide, Angew. Chem. Int. Ed. 42 (2003) 4908.
[17] X.T. Hong, Z.P. Wang, W.M. Cai, F. Lu, J. Zhang, Y.Z. Yang, N. Ma, Y.J. Liu, Visible-light-activated nanoparticle photocatalyst of iodine-doped titanium dioxide, Chem. Mater. 17 (2005) 1548.
[18] J.C. Yu, J. Yu, W.K. Ho, Z. Jiang, L. Zhang, Effects of F doping on the photocatalytic activity and micro structures of nanocrystalline TiO_2 powders, Chem. Mater. 14 (2002) 3803–3816.
[19] N. Todorova, T. Giannakopoulou, T. Vaimakis, C. Trapalis, Structure tailoring of fluorine-doped TiO_2 nanostructured powders, Mater. Sci. Eng. B 152 (2008) 50–54.
[20] W. Zhao, W.H. Ma, C.C. Chen, J.C. Zhao, Z.G. Shuai, Efficient degradation of toxic organic pollutants with Ni_2O_3/TiO_2–xBx under visible irradiation, J. Am. Chem. Soc. 126 (2004) 4782.
[21] Z.Q. He, X. Xu, S. Song, L. Xie, J.J. Tu, J.M. Chen, B. Yan, A visible light-driven titanium dioxide photocatalyst codoped with lanthanum and iodine: an application in the degradation of oxalic acid, J. Phys. Chem. C 112 (2008) 16431.
[22] H. Kato, A. Kudo, Visible-light-response and photocatalytic activities of TiO_2 and $SrTiO_3$ photocatalysts codoped with antimony and chromium, J. Phys. Chem. B 106 (2002) 5029–5034.
[23] H.G. Yang, H.C. Zeng, Preparation of hollow anatase TiO_2 nanospheres via Ostwald ripening, J. Phys. Chem. B 108 (2004) 3492–3495.
[24] N. Todorova, T. Giannakopoulou, T. Vaimakis, J. Yu, C. Trapalis, Preparation of fluorine-doped TiO_2 photocatalysts with controlled crystalline structure, Int. J. Photoenergy, doi:10.1155/2008/534038.
[25] X. Jiang, L. Yang, P. Liu, X. Li, J. Shen, The photocatalytic and antibacterial activities of neodymium and iodine doped TiO_2 nanoparticles, Colloids Surf. B: Biointerfaces 79 (2010) 69–74.
[26] F. Ran, L. Miao, S. Tanemura, M. Tanemura, et al., Effect of annealing temperature on optical properties of Er-doped ZnO films prepared by sol–gel method, Mater. Sci. Eng. B 148 (2008) 35–39.
[27] E. Sanchez, T. Lopez, Effect of the preparation method on the band gap of titania and platinum–titania sol–gel materials, Mater. Lett. 25 (1995) 271–275.
[28] A.M. Czoska, S. Livraghi, M. Chiesa, E. Giamello, et al., The nature of defects in fluorine-doped TiO_2, J. Phys. Chem. C 112 (2008) 8951–8956.
[29] X.T. Hong, Z.P. Wang, Visible light activated nanoparticle photocatalyst of iodine doped titanium dioxide, Chem. Mater. 17 (2005) 1548–1552.
[30] D. Li, H. Haneda, S. Hishita, N. Ohashi, N.K. Labhsetwar, Fluorine doped TiO_2 powders prepared by spray pyrolysis and their improved photo catalytic activity for decomposition of gas-phase acetaldehyde, J. Fluorine Chem. 126 (2005) 69–77.
[31] C. Di Valentin, E. Finazzi, G. Pacchioni, Density functional theory and electron paramagnetic resonance study on the effect of N–F codoping of TiO_2, Chem. Mater. 20 (2008) 3706–3714.
[32] G. Cao, Y. Li, Q. Zhang, H. Wang, Synthesis and characterization of La_2O_3/TiO_2–xFx and the visible light photocatalytic oxidation of 4-chlorophenol, J. Hazard. Mater. 178 (2010) 440–449.
[33] C. Wang, Y. Ao, P. Wang, J. Hou, J. Qian, Preparation, characterization and photocatalytic activity of the neodymium-doped TiO_2 hollow spheres, Appl. Surf. Sci. 257 (2010) 227–231.
[34] C. Wen, Y.-J. Zhu, T. Kanbara, H.-Z. Zhu, C.-F. Xiao, Effects of I and F codoped TiO_2 on the photocatalytic degradation of methylene blue, Desalination 249 (2009) 621–625.
[35] J. Wang, D.N. Tafen, J.P. Lewis, Z.L. Hong, A. Manivannan, M.J. Zhi, M. Li, N.Q. Wu, Origin of photocatalytic activity of nitrogen-doped TiO_2 nanobelts, J. Am. Chem. Soc. 131 (2009) 12290–12297.
[36] T. Tachikawa, S. Tojo, K. Kawai, M. Endo, M. Fujitsuka, T. Ohno, K. Nishijima, Z. Miyam-oto, T. Majima, Photocatalytic oxidation reactivity of holes in the sulfur and carbon-doped TiO_2 powders studied by time-resolved diffuse reflectance spectroscopy, J. Phys. Chem. B 108 (2004) 19299–19306.